Rock and Soil Mechanics

Volume 44 | Issue 3 Article 5

7-21-2023

Deformation and load transmission mechanism of prestressed reinforced embankment subjected to rockfall impacts

Shu-wen MA
School of Civil Engineering, Chongqing University, Chongqing 400045, China, Department of Architectural & Engineering, Chongqing Industry Polytechnic College, Chongqing 401120, China

Liang LU
School of Civil Engineering, Chongqing University, Chongqing 400045, China, Key Laboratory of New Technology for Construction of Cities in Mountain Area, Ministry of Education, Chongqing 400045, China, National Joint Engineering Research Center of Geohazards Prevention in the Reservoir Areas, Chongqing University, Chongqing 400045, China

Zong-jian WANG
College of River & Ocean Engineering, Chongqing Jiaotong University, Chongqing 400074, China

Jing-tian WANG
School of Civil Engineering, Chongqing University, Chongqing 400045, China, Key Laboratory of New Technology for Construction of Cities in Mountain Area, Ministry of Education, Chongqing 400045, China

See next page for additional authors

Deformation and load transmission mechanism of prestressed reinforced embankment subjected to rockfall impacts

Authors

Shu-wen MA, Liang LU, Zong-jian WANG, Jing-tian WANG, and Lan-xing LI

Rock and Soil Mechanics 2023 44(3): 799−809 ISSN 1000−7598
https: //doi.org/10.16285/j.rsm.2022.5471 http://rocksoilmech.researchcommons.org/journal

Deformation and load transmission mechanism of prestressed reinforced embankment subjected to rockfall impacts

MA Shu-wen[1, 2], LU Liang[1, 3, 4], WANG Zong-jian[5], WANG Jing-tian[1, 3], LI Lan-xing[1, 3]

1. School of Civil Engineering, Chongqing University, Chongqing 400045, China
2. Department of Architectural & Engineering, Chongqing Industry Polytechnic College, Chongqing 401120, China
3. Key Laboratory of New Technology for Construction of Cities in Mountain Area, Ministry of Education, Chongqing 400045, China
4. National Joint Engineering Research Center of Geohazards Prevention in the Reservoir Areas, Chongqing University, Chongqing 400045, China
5. College of River & Ocean Engineering, Chongqing Jiaotong University, Chongqing 400074, China

Abstract: The prestressed reinforced soil structure was proposed to solve the problem of large-area depressions of soil highways under rockfall impacts in remote mountain areas. Comparative model tests for prestressed reinforced soil embankment and traditional soil embankment were conducted to explore the deformation performance, mechanical response, and load transmission mechanism of both embankments under rockfall impacts. The results show that the size of pits formed in prestressed reinforced soil embankment is significantly smaller than that in traditional soil embankment, which reflects the good impact deformation resistance of prestressed reinforced soil embankment. The embankment stiffness increases with the increase of impact times, resulting in the change of the time history of impact-induced additional stress in the embankment from “parabolic single peak” to “double peak”, and the “double peak” in the prestressed reinforced soil embankment occurs earlier than that in the traditional soil embankment. The duration of rockfall impact on the prestressed reinforced soil embankment is less than that on the traditional soil embankment, and the distribution of the impact on the prestressed reinforced soil embankment is more uniform, indicating that the prestressed reinforced soil embankment is more conducive to the impact diffusion. In addition, the internal impact load transmission ratio for prestressed reinforced soil embankment increases first and then decreases with the increase of impact times, which is consistent with the deformation law of reinforcement structure. The pit sizes corresponding to various impact times are predicted by the Levenberg-Marquardt optimization algorithm, which can provide reference for the engineering application of prestressed reinforced soil embankment and early warning in collapse disaster prone areas.

Keywords: rockfall impact; prestressed reinforced soil embankment; impact deformation; additional stress; impact duration; impact transmission ratio

1 Introduction

As one of the common and serious geological hazards in mountain areas, the rockfall hazard has the characteristics of massive devastation, high speed, random movement route, and irregular volume[1−3]. Due to poor construction conditions and slow economic development, deep depression deformations of highways in remote mountain areas are frequently caused by rockfall impacts, and the maximum diameter of rockfall can reach 3.8 m[4], which not only affects normal traffic but also increases the difficulty of rescue activities in major hazards, and even causes serious casualties and economic losses[5]. Traditional impact prevention measures for highway pavements include the cushion method with soil replacement, dynamic compaction method, and temporary method, but their applications in remote mountain highways are limited due to the demand for huge construction machinery, lengthy construction period, and high repair costs. “Reinforced soil technique” has become an important technical means to prevent highway rockfall hazards for its benefits in significant global highway stability improvement[6], excellent deformation resistance[7], high dynamic flexibility and ductility[8], strong impact resistance, high strength and stiffness–mass ratio[9], and low cost, and this technique has been widely used in earthquake-prone regions such as Japan[10−14]. For example, a reinforced soil embankment built in a mountain area in Japan successfully intercepted rockfalls of various sizes totaling 76 t during a sudden large-scale rockfall hazard[4]. However, the deformation characteristics of high flexibility, high ductility, and low stiffness lead to local large-scale depression deformations of the reinforced soil embankment under rockfall impacts. Although the global collapse of the embankment is prevented, the depressed embankment loses its resistance capacity to another such large-scale rockfall impact.

Received: 8 April 2022 Accepted: 5 May 2022
This work was supported by the National Natural Science Foundation of China(52178314) and the Graduate Scientific Research and Innovation foundation of Chongqing(CYB22031).
First author: MA Shu-wen, born in 1992, PhD candidate, focusing on early warning and prevention of geotechnical engineering disasters.
E-mail: mashuwenwen@163.com
Corresponding author: LU Liang, female, born in 1978, PhD, Associate Professor, PhD supervisor, mainly engaged in teaching and research on geotechnical engineering disasters. E-mail: luliangsky@163.com

Therefore, a reinforced embankment structure with strong deformation resistance is urgently needed.

The proposal of "prestressed reinforced soil"[15] can successfully address the aforementioned concerns and was first applied in Japan[10, 16]. For the reinforced soil structure, the applied prestress can effectively enhance its deformation resistance[17], leading the overlying load to be distributed over a wider region. Roh et al.[18] investigated the effects of reinforcement material and prestress on stress–strain characteristics of reinforced saturated clay through plane strain compression tests, and the results show that the structural stiffness exhibits no remarkable growth trend with increasing reinforcement material number but increases significantly with rising prestress. Shivashankar et al.[19] established an analytical model to predict the bearing capacity of prestressed geosynthetic reinforced granular beds overlying weak soil. Jayamohan and Shivashankar[20] and Lovisa et al.[21] examined the deformation characteristics and bearing capacities of permanent prestressed reinforced cushions through model tests. Du et al.[22] explored the technical principle of prestressed carbon fiber reinforced plastic (CFRP) reinforced soil through triaxial tests and introduced the concept of "pseudo-cohesion", which serves as a reference for the mechanical analysis of prestressed reinforced soil structure. As a result, the prestressed reinforced technique not only ensures structural deformation stability but also exhibits outstanding engineering adaptability. However, the impact deformation resistance, internal mechanical response, and load transmission mechanism of prestressed reinforced embankment are inadequately revealed.

To explore the deformation resistance, mechanical response law, and load transmission mechanism of prestressed reinforced embankment under rockfall impacts, comparative model tests for prestressed reinforced soil embankment and plain fill embankment were designed and conducted. Based on the Levenberg-Marquardt optimization algorithm and model test data, the functional relationships between impact times and pit sizes were fitted, which can provide a reference for the application of prestressed reinforced soil structure in highway engineering.

2 Impact model test

Based on comparison principles, rockfall impact resistance capacities of traditional plain fill embankment and prestressed reinforced soil embankment were compared by designing diverse model test conditions, and the comparison results were further used to examine the deformation and dynamic response characteristics of prestressed reinforced soil embankment under the rockfall impact.

2.1 Test model

In the model test, a concrete hard subgrade and a soft soil subgrade were separately filled to simulate the bridge culvert and its nearby highway subgrade, and then a traditional plain fill or prestressed reinforced soil embankment was constructed above the filling subgrades to complete the entire test model construction, as depicted in Fig. 1. The prestressed reinforced embankment is composed of reinforced inclusion and prestressed components. The reinforced inclusion consists of filling and reinforcement materials, while the prestressed components comprise gaskets, anchorages, and tension members. The tension member is fastened at its top by the anchorage after passing through the lower gasket, the reinforced inclusion, and the upper gasket. The anchorage can exert pressure on the reinforced inclusion by moving downward along the axial direction of the tension member. The compressed reinforced inclusion deforms and applies restricting pressure to the filling material until the prestress exertion is finished. A prestressed reinforced soil highway[23−24] in Ibaraki, Japan was selected as the test prototype. The prototype highway has a width of 3 m, a height of 600 mm for the roadbed made up of three layers of prestressed reinforced soil structures, and a spacing of 450 mm for the prestressed components. For the prototype highway, the prestress was applied to the highway structure by controlling the axial strain of the prestressed components, but the concrete axial strain values (prestrain) were not described in detail. The prestrain affects the bending stiffness of prestressed reinforced soil structure, and the effect is prominent when the intended prestrain range is within 0.1%[25]. Therefore, the prestrain corresponding to the elongation ratio is set to 0.1% in the model tests. In the prestressed reinforced embankment model, there are 17 measuring points including 8 strain gauges and 9 horizontally arranged earth pressure boxes. For comparison convenience, the position and number of earth pressure box in the traditional plain fill embankment model are consistent with those in the prestressed reinforced embankment model.

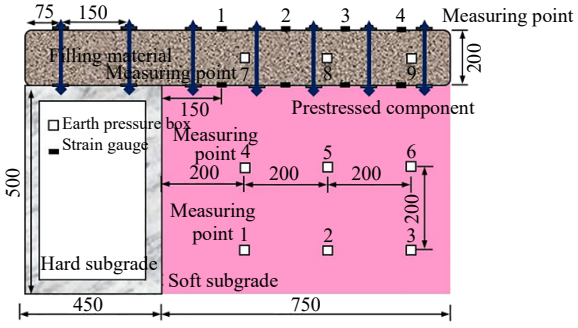

Fig. 1 Schematic diagram of model test (unit: mm)

The drop hammer loading system was employed to produce impact loads to replicate the impact effects of free falling rockfall on the embankment. The loading system is composed of a swing rope, a solid ball, and a gantry crane, as displayed in Fig. 2. A concrete solid ball weighing 32.5 kg and having a diameter of around 300 mm was picked to simulate the rockfall. According to the size of the rockfall impact loading system, the ball radius, and the test model height, the height of each rockfall impact was set to 3 m. Depending on the test site conditions, the gantry crane size (the permitted embankment width is 1.2 m), and the prototype size, the maximum attainable similarity ratio of 1:3 was determined as the geometric similarity ratio for designing the test model. Based on the similarity principle[26], the similarity relationships of the model tests are listed in Table 1.

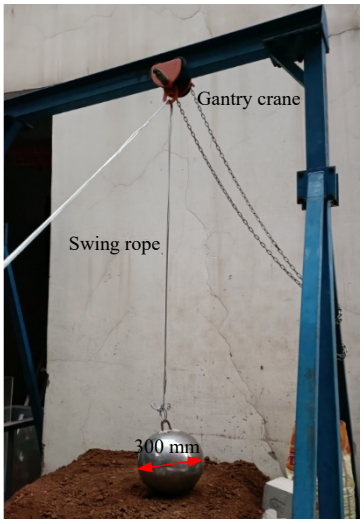

Fig. 2 Loading system for rockfall impact

Table 1 Similarity ratios for model tests

Length L /m	Acceleration a /(m • s^{-2})	Unit weight γ /(N • m^{-3})	Time t /s	Velocity v /(m • s^{-1})	Mass m /kg	Stress σ /kPa	Young's modulus E /kPa	Energy W /J
1/3	1	1	$1/3^{1/2}$	$1/3^{1/2}$	1/27	1/3	1/3	1/162

2.2 Test scheme and material

2.2.1 Test scheme

In this model test, the prestressed reinforced soil embankment was designated as the target group, whereas the plain fill embankment was designated as the control group. When the depth of the embankment pit caused by the rockfall impact reached 15 cm (the restored actual pit depth in accordance with the similarity ratio is 45 cm, which was greater than the average tire radius) in the preliminary test, the impact times were 30 and the pavement was considered unsuitable for traffic in such condition. As a consequence, 30 cycles of rockfall impacts were performed on the embankment model.

2.2.2 Test material

In practical engineering, the typical tensile strength range of geosynthetics is 50−120 kN /m[27]. Based on the similarity relationship, the nylon gauze was adopted to simulate the reinforcement material, and its tensile strength is 30 kN /m according to the standard tensile test findings. Self-locking nylon ties were selected as the prestressed components and anchorages, and clay was selected as the filling material, whose mechanical properties are given in Table 2.

Before the model test, strain gauges need to be pasted on the nylon gauze. The strain gauge and the nylon gauze were initially glued together, and then the bonding areas along with their surrounding areas were subsequently coated with adhesive tape for secondary protection. The insulation shielding was carefully carried out to prevent exposed wire connections from contacting with other distracting items, resulting in erroneous data gathering, as represented in Fig. 3.

Table 2 Physical and mechanical parameters of clay

Compressive modulus /MPa	Natural Mass density /(g • cm^{-3})	Natural water content /%	Specific gravity G_s	Plastic limit /%	Liquid limit /%	Plastic index	Cohesion /kPa	Internal friction angle /(°)	Nonuniformity coefficient	Curvature coefficient	D_{60} /mm	D_{30} /mm	D_{10} /mm
8.1	1.86	15.3	2.635	15.5	27.8	12.3	16.3	28.1	1.8	1.1	0.87	0.63	0.37

Note: D_{60}, D_{30}, and D_{10} are particle sizes corresponding to 60%, 30%, and 10% finer by mass.

The Donghua 5921 dynamic data acquisition and analysis system was employed to collect test data from the measuring elements, as shown in Fig. 4.

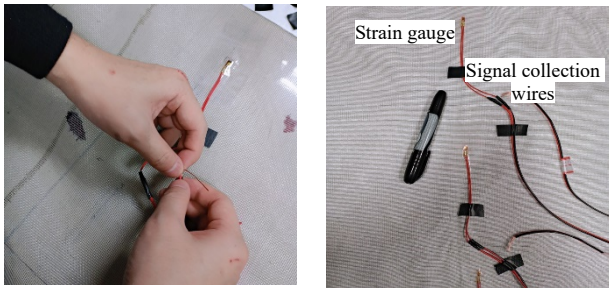

(a) Wiring process (b) Wiring completion

Fig. 3 Fixing and wiring of strain gauges

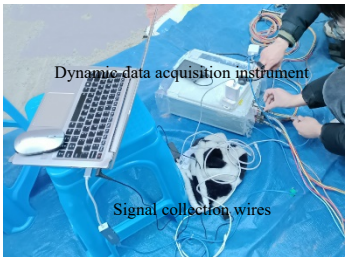

Fig. 4 Dynamic data acquisition instrument

2.3 Test steps

(1) Soft and hard subgrade construction. The hard subgrade was casted with cement concrete, and the soft subgrade was filled using layers of clay with relative compaction of 80% through the pluviation.

(2) Measuring elements arrangement. The earth pressure boxes were arranged according to the distribution map of measuring elements, as marked in Fig. 1.

(3) Bottom gasket and self-locking nylon ties of prestressed components installation. The prestressed component positions were first labeled on the nylon gauze, followed by the installation of the bottom gasket and self-locking nylon ties.

(4) Embankment construction. One side of nylon gauze with gasket and nylon tie was first laid on the subgrade, then the clay was filled and tamped on the laid nylon gauze, and lastly the reinforcement material was repacked and sewed.

(5) Prestress loading. The prestrain of 0.1% was applied at the reserved loading position, and the redundant parts of self-locking nylon ties were cut off following the prestrain stabilization.

(6) Loading. The solid ball was elevated to the highest point of the drop hammer system, then relaxed, and its free falling movement was utilized to imitate the rockfall impact.

(7) Data acquisition. Before each rockfall impact, the data acquisition instrument was cleared to eliminate the interference from the data measured in the static state on the test results. The test processes are presented in Fig. 5.

3 Test results and analysis

3.1 Embankment surface deformation

To demonstrate the impact deformation resistance and the dissipation effect on rockfall impact energy of prestressed reinforced embankment and plain fill embankment, the collected data from the first five impact tests for plain fill embankment were selected, while the collected data from the first eight impact tests for prestressed reinforced embankment were chosen because the pit depth in the prestressed reinforced embankment under the rockfall impact was far lower than that in the plain fill embankment.

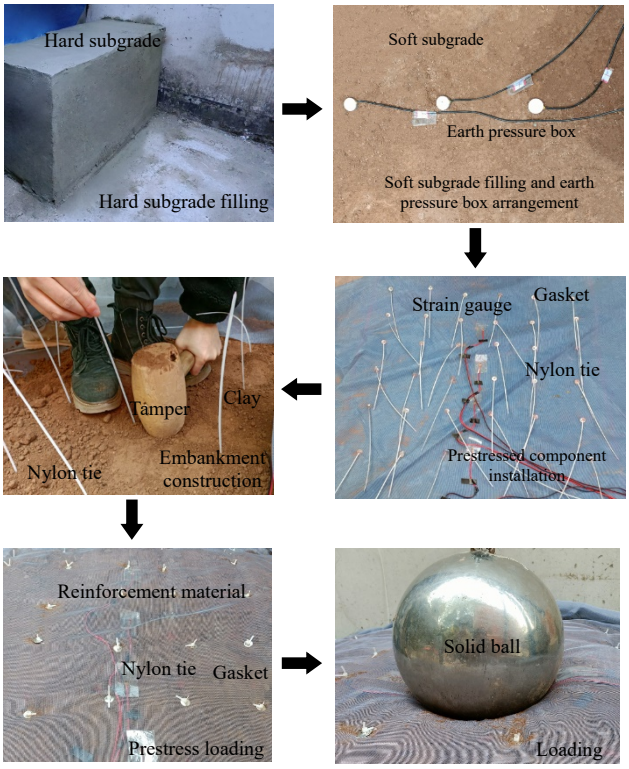

Fig. 5 Test processes

The surface deformations of plain fill embankment after solid ball impact are illustrated in Fig. 6. As the impact times increase, the pit sizes also grow with growth rates

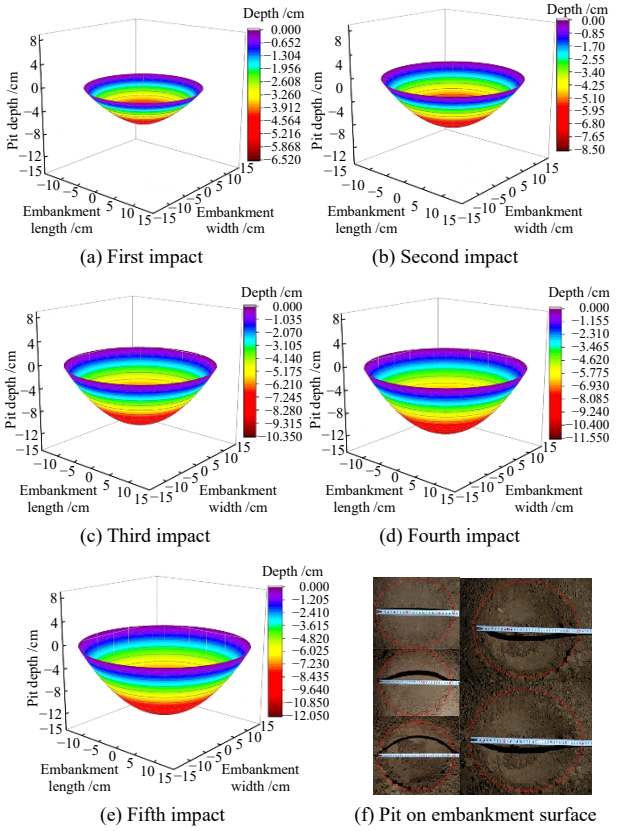

Fig. 6 Surface deformation of plain fill embankment under cyclic impacts

https://rocksoilmech.researchcommons.org/journal/vol44/iss3/5
DOI: 10.16285/j.rsm.2022.5471

of 30.8%, 21.2%, 11.7%, and 4.3% for pit depth and 20.0%, 6.7%, 6.2%, and 5.8% for pit radius. The growth rate of pit size decreases with the increase of impact times.

As illustrated in Fig. 7, the pit depth and radius of prestressed reinforced soil embankment under the rockfall impact also grow with increasing impact times, with growth rates of 28.6%, 20.0%, 19.0%, 6.1%, 5.8%, 2.7%, and 2.6% for pit depth and 19.0%, 12.0%, 3.6%, 2.8%, 2.0%, 1.3%. and 0.7% for pit radius. Compared to the plain fill embankment, the growth rates of pit sizes for the prestressed reinforced soil embankment under the rockfall impact are significantly reduced, reflecting the good deformation resistance of prestressed reinforced soil embankment, which is conducive to the uniform diffusion of upper impact loads. Furthermore, the pit depth of prestressed reinforced soil embankment after 8 impacts is still lower than that of plain fill embankment after 2 impacts, indicating the remarkable deformation energy absorption and diffusion energy dissipation characteristics of prestressed reinforced soil embankment.

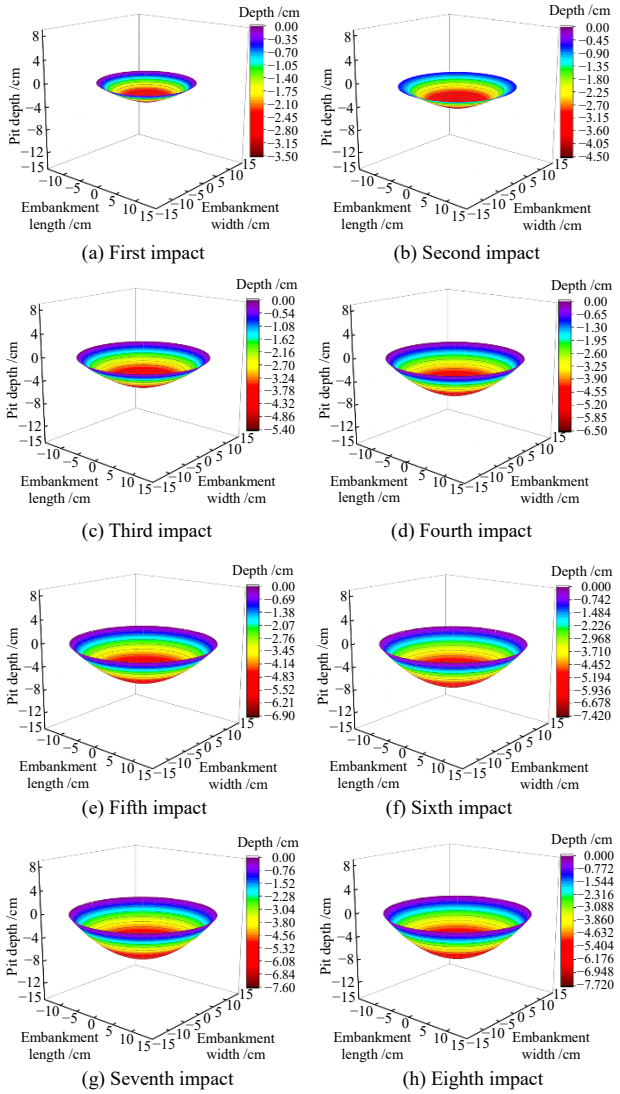

Fig. 7 Surface deformation of prestressed reinforced soil embankment under cyclic impact

The Levenberg-Marquardt optimization algorithm is commonly used in nonlinear fitting of discrete data[28–29] with strong robustness and broad convergence domain. Based on the Levenberg-Marquardt optimization algorithm and the collected data from the first 10 impact tests, the nonlinear fitting of the pit depth and radius in the Exponential function form was performed using the Asymptotic model through the nonlinear curve fitting tool in Origin 2018. The obtained function relationships between impact times (x) and pit depth (y_1) as well as pit radius (y_2) under the two working conditions are as follows:

Plain fill embankment:

$$y_1 = 13.96 - 10.68 \times 0.70^x \quad (1)$$

$$y_2 = 19.31 - 9.84 \times 0.68^x \quad (2)$$

Prestressed reinforced soil embankment:

$$y_1 = 8.60 - 6.85 \times 0.76^x \quad (3)$$

$$y_2 = 15.79 - 9.08 \times 0.59^x \quad (4)$$

According to Eqs. (1) and (3), the predicted maximum pit depths of plain fill embankment and prestressed reinforced embankment are 13.96 cm and 8.60 cm, and the corresponding impact times are 22 and 18, which are consistent with the maximum depths (13.25 cm and 8.51 cm) of the test model under 22 impacts. Similarly, the maximum pit radii predicted by Eqs. (2) and (4) under the two working conditions are 19.31 cm and 15.79 cm, and the corresponding impact times are 22 and 15, which are consistent with the maximum pit radii (19.05 cm and 15.37 cm) of the test model under 22 impacts. The predicted impact times corresponding to the maximum pit radius are smaller than the test results, indicating that the prediction method can conservatively forecast the impact times that the embankment can withstand, which aids in hazard assessment and prevention. In view of the predicted maximum pit sizes, the prestressed reinforced soil embankment offers substantial benefits in controlling impact deformation.

According to the test findings, the reinforcement materials under the rockfall impact absorb part of the impact energy through their own elastic and plastic deformations, which is reflected by the suspended gap between reinforcement material and its underlying filling material after the rockfall is removed, as displayed in Fig. 8(a). The maximum depth distributions of the pit formed by filling and reinforcement materials are plotted in Fig. 8(b). The depression depth of the reinforcement material is substantially smaller than that of the filling soil owing to the superior deformation energy absorption and tensile properties of the reinforcement material. Moreover, the reinforcement material is low in cost, simple in production process, and convenient for transportation, making it ideal

for mountain areas with frequent rockfall hazards.

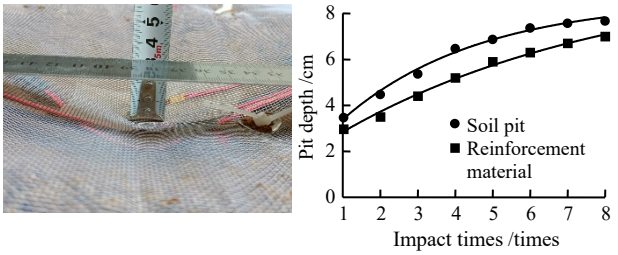

(a) Physical image (b) Comparison of reinforcement material and filling soil

Fig. 8 Separation of reinforcement structure from soil

3.2 Additional stress response

The additional stress distributions inside the model under the two working conditions are described in Fig. 9. The rockfall impact is a sudden instantaneous impact process with an action time counting in milliseconds. When the impact times are fewer, the embankment filling material is rapidly compressed under the rockfall impact, causing a “parabolic single peak” distribution of the additional stress. As the impact times rise, the filling material becomes more compact, the contact between the filling materials becomes more solid, and the additional stress shows a “double peak” distribution, which is represented by rockfall rebound and the subsequent secondary impact on the embankment. In comparison to the “double peak” phenomenon at the fifth impact under the plain fill embankment condition, the “double peak” phenomenon occurs at the fourth impact under the pre-stressed reinforced soil embankment condition because of its greater structural stiffness resulting from its excellent prestressed reinforcement characteristics. With the increase of impact times, the developed tensile properties and lateral constraints of reinforcement materials lead to much more enhancement in the stiffness of the prestressed reinforced soil embankment than that of the plain fill embankment, so the secondary rockfall impact occurs earlier for the prestressed reinforced soil embankment. As a semi-rigid structure between flexible and rigid structures,

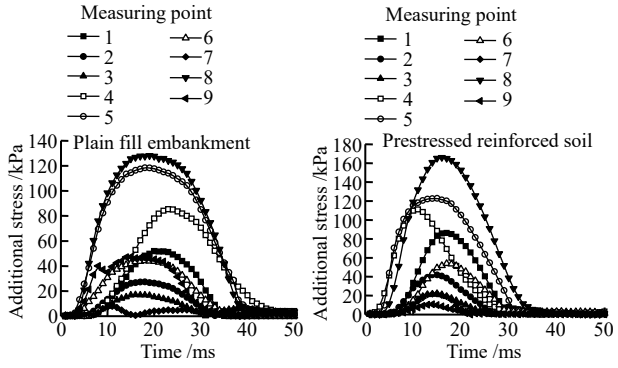

(a) First impact

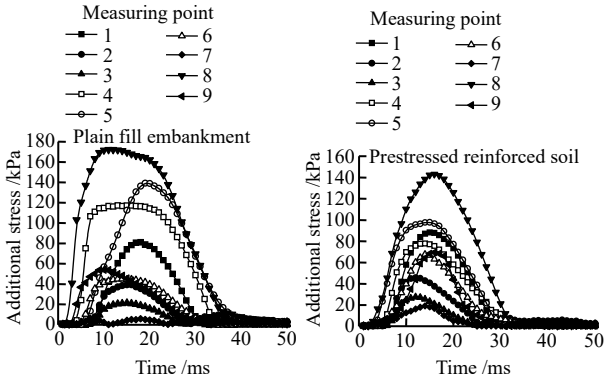

(b) Second impact

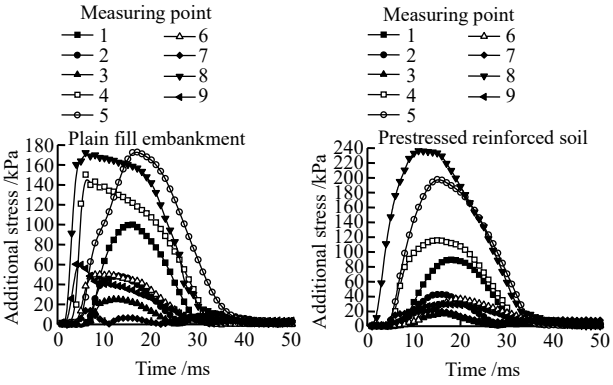

(c) Third impact

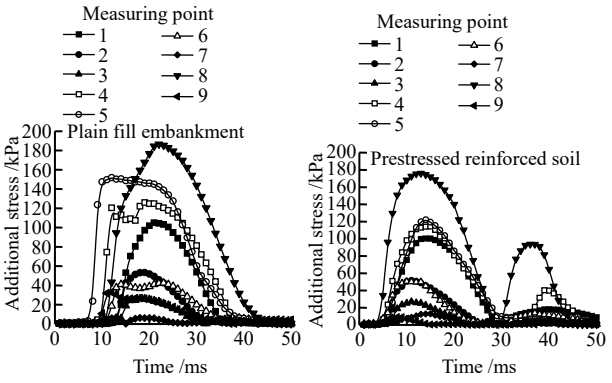

(d) Fourth impact

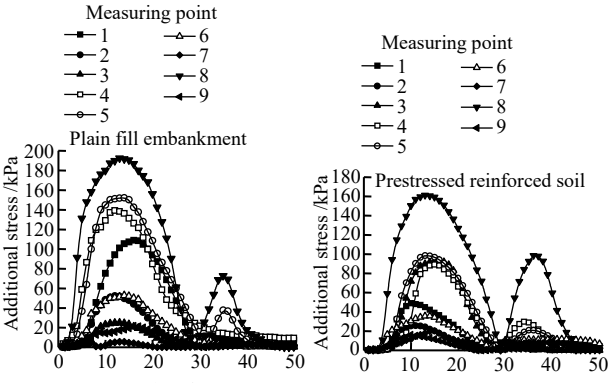

(e) Fifth impact

Fig. 9 Time history of additional stress at each measuring point

the prestressed reinforced embankment has good buffering and energy dissipation characteristics, and it can make the rockfall rebound ahead of that occurs in the plain fill embankment to disperse the impact energy, extending the buffering time to reduce the impact deformation and achieve the energy dissipation (Fig. 8). For measuring point 8, when the impact times are fewer than 4, the compactness of filling material inside the embankment grows under cyclic rockfall impacts, and the pit develops larger and larger, resulting in a decrease in the distance from the impact point to measuring point 8 and an increase in peak additional stress. As the impact times continue to increase, the lateral deformation of the embankment filling material under the rockfall impact is limited by the repacked reinforcement materials, resulting in the increasing stiffness of prestressed reinforced embankment and the rockfall rebound, and the secondary energy dissipation characteristics of the structure realize their full potential, resulting in a decrease in the peak additional stress.

The average maximum additional stress distributions at each measuring point under the two working conditions are demonstrated in Fig. 10. The additional stress under the prestressed reinforced embankment condition is lower than that under the plain fill embankment condition. The prestressed reinforced embankment has a higher rigidity, which allows the impact load to be transmitted over a greater distance. The pre-constraint effect of the reinforcement material and the friction effect of reinforcement–soil balance part of the impact load, and the tensile properties of the reinforcement material are fully developed due to the pre-deformation caused by its earlier stretching, thus balancing part of the additional stress.

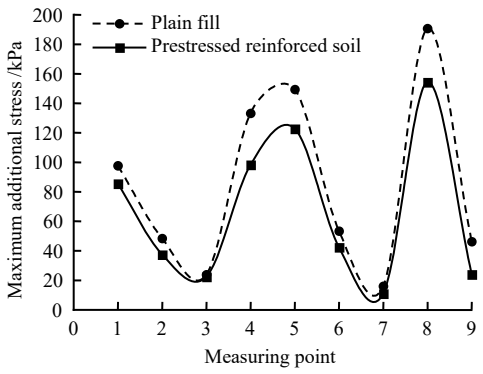

Fig. 10 Maximum additional stress at each measuring point

3.3 Reinforcement material strain

The reinforcement material strain under the prestressed reinforced embankment condition is shown in Fig. 11, and the strain of the reinforcement material on the top layer is significantly larger than that on the bottom layer. The rockfall initially strikes and collides with the reinforcement material on the top layer, and since the tensile properties of the reinforcement material balance part of the impact load, the impact load on the reinforcement material on the bottom layer is greatly decreased. Since the impact point is between measuring points 2 and 3 and closer to measuring point 3, the impact load and reinforcement material deformation at measuring point 3 are greater than those at measuring point 2, resulting in the greatest additional stress near measuring point 3, which is consistent with the result in Section 3.2 that the greatest additional stress is at measuring point 8. Similarly, the reinforcement material strain at measuring point 4 is larger than that at measuring point 1 because the distance between measuring point 4 and the impact point is shorter.

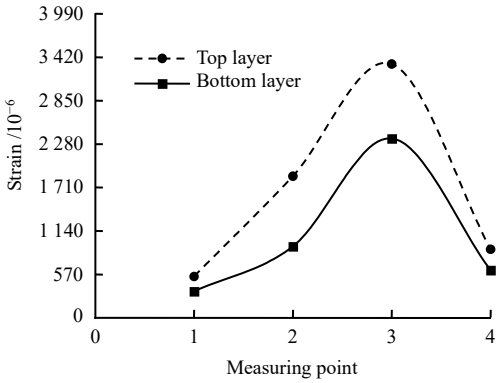

Fig. 11 Strains of reinforcement structure under different conditions

3.4 Impact duration

To explore the relationship between rockfall impact duration and impact times, the relationship curves under the plain fill and prestressed reinforced soil conditions are drawn in Figs 12 (a) and 12 (b). With the increase of impact times, the impact durations under the two working conditions are reduced, because the compactness of embankment filling material increases with the increasing impact times, shortening the transmission path of impact load. Compared to the plain fill embankment condition, the duration distribution at each measuring point is more uniform under the prestressed reinforced soil embankment condition. The prestressed reinforced technique allows for the tensile properties of the reinforcement material to be exhibited in advance, eliminating the filling material compression and improving the reinforced embankment stiffness in advance, which is conducive to the diffusion of the upper impact load and its uniform transmission to the lower subgrade. Since measuring point 8 is closest to the rockfall impact point, the impact load and area there are the largest, resulting in a longer duration. Similarly, the duration at measuring point 5 on the same vertical

line as measuring point 8 is longer than that at measuring point 2, and the duration at the measuring point on the same horizontal layer decreases as the distance from the impact point increases.

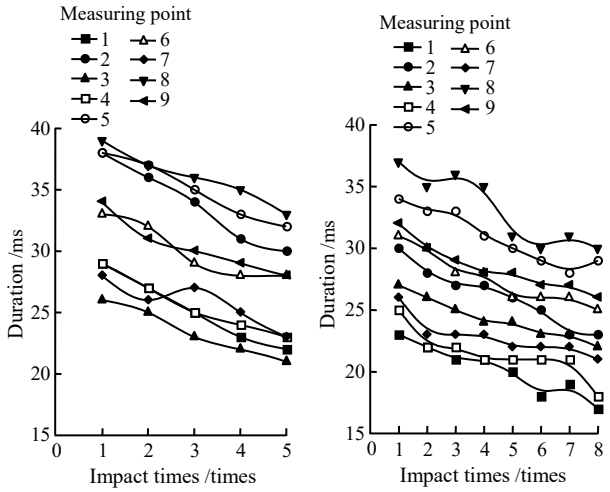

Fig. 12 Relationship between impact duration and impact times

To compare the duration difference between the plain fill and prestressed reinforced soil embankment conditions, the average duration distribution curve at each measuring point is plotted in Fig. 13. The rockfall impact duration under the plain fill embankment condition is longer than that under the prestressed reinforced soil embankment condition. Because of the same reason stated above, the durations at measuring points 2, 5, and 8 are longer than those at other measuring points. In addition, the durations at measuring points 1, 4, and 7 are shorter than those at measuring points 3, 6, and 9. The measuring points 1, 4, and 7 are near the hard subgrade, which increases the compactness of filling material under the rockfall impact and the lateral constraint of hard subgrade, allowing the impact load to diffuse more quickly. However, the filling materials near the measuring points 3, 6, and 9 become loose under the rockfall impact because they are not subjected to the rigid lateral constraint of the hard subgrade, which is not conducive to impact load transmission.

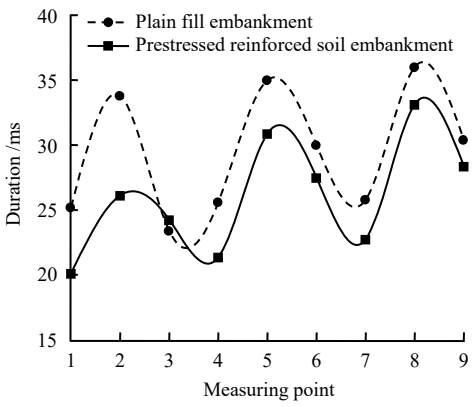

Fig. 13 Impact duration at each measuring point

3.5 Impact transmission ratio

The transmission ratio T_r is closely related to the earth pressure σ and the impact pressure p[30], and its specific expression is

$$T_r = \left(\frac{\sigma}{p}\right)_{max} \tag{5}$$

The expression of the maximum impact pressure p_{max} is

$$p_{max} = \frac{m a_{max}}{A} \tag{6}$$

where m denotes the falling ball weight (kg); A is the maximum contact area between the falling ball and the embankment (0.141 m^2); a_{max} is the maximum impact acceleration. *According* to the momentum conservation law, the integration of impact acceleration on impact time t is the impact velocity v_0[31], and the impact velocity is proportional to the square root of the falling height h. Therefore, the maximum impact acceleration can be calculated by

$$\int a_{max} \mathrm{d}t = \sqrt{2gh} \tag{7}$$

where g is the gravity acceleration (m /s^2).

Then, the rockfall impact transmission ratio can be obtained by substituting Eqs. (7) and (6) into Eq. (5).

The transmission ratios estimated from the data at measuring points (measuring points 8, 5, and 2) positioned on the same vertical line as the impact point are summarized in Fig. 14. The impact transmission ratio falls from top to bottom, which conforms to the principle of impact energy dissipation. Compared with the plain fill embankment condition, the impact transmission ratio at each measuring point is lower under the prestressed reinforced soil embankment condition, which reflects the excellent characteristics of the prestressed reinforced embankment including flexible deformation energy absorption and semi-rigid energy diffusion. As a result, the prestressed reinforced soil embankment is more conducive to rockfall impact absorption, transmission, and diffusion.

In contrast to other measuring points, the impact transmission ratio at measuring point 8 in the prestressed reinforced embankment exhibits a “first rise and then decline” trend with the increase of impact times, as depicted in Fig. 15. With fewer impact times, the depression deformation of the embankment is mostly used to absorb energy,

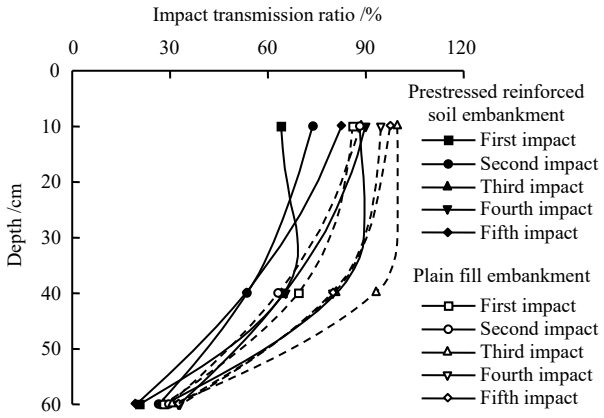

Fig. 14 Variation of impact transmission ratio along depth

and the embankment deformation is determined by the reinforcement material deformation. As the impact times rise, the reinforcement material deformation increases and the distance from the impact point to measuring point 8 decreases, resulting in a shorter impact transmission path and an increase in transmission ratio. As the impact times continue to increase, so does the reinforcement material deformation. The restraint effect of the reinforcement material on the embankment filling material reaches the maximum through lateral swelling deformation, the embankment stiffness reaches its maximum, and the impact energy dissipation changes from the original energy absorption through deformation to the energy diffusion, as verified by the rockfall rebound phenomenon in the model test. Starting from the fifth impact, energy dissipation is mostly accomplished by diffusion in structure, and the impact compaction causes the diffusion range to rise, resulting in a drop in transmission ratio. Because the other measuring points are in a clay environment, their compactness increases as the impact times rise, and the distances between them and the impact point decrease, increasing the impact transmission ratio.

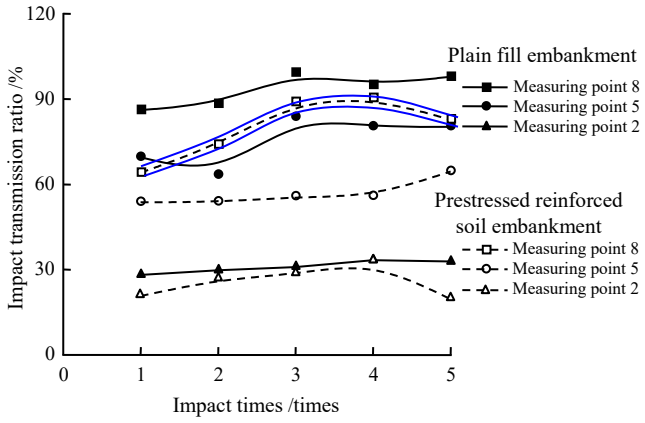

Fig. 15 Relationship between impact transmission ratio and impact times

3.6 Discussion

According to the test findings: (a) The prestressed reinforced material can display the tensile properties and lateral restraint effects in advance, pre-eliminating the filling material compression and limiting the lateral embankment deformation, which significantly increases the structural stiffness and reduces the impact deformation[32]. (b) With the increase of impact times, the prestressed reinforced embankment transitions from a flexible to a semi-rigid structure. Part of the impact energy is absorbed by structural deformation, and part of the energy is diffused through the structure, which promotes the dispersion and transmission of impact load[33]. Only the impact deformation resistance of the plain fill embankment was compared to that of the prestressed reinforced embankment, and many factors affecting the impact deformation resistance were not investigated, such as tensile strength and arrangement of reinforcement material, prestress level, prestressed component spacing, and reinforcement–soil interaction characteristics[16–20]. Therefore, conducting special research on the influence of various factors on the impact deformation resistance of prestressed reinforced embankment has significant research significance and practical application value.

4 Conclusion

To investigate the deformation resistance, mechanical response, and load transmission mechanism of prestressed reinforced embankment under the rockfall impact, comparative model tests were designed and implemented for prestressed reinforced embankment and plain fill embankment. The major conclusions are as follows:

(1) Under the rockfall impact, the sizes of pits formed in the prestressed reinforced soil embankment are significantly smaller than those in the plain fill embankment, indicating the good impact deformation resistance of the prestressed reinforced embankment. Based on the Levenberg-Marquardt optimization algorithm and the model test data, the nonlinear fitting of the pit sizes in the form of exponential functions is carried out using the Asymptotic model, and the prediction equations for the pit sizes based on the impact times were generated. The prediction results are consistent with the test results, which can provide a reference for early warning in collapse hazard-prone areas.

(2) With the increase of impact times, the distribution law of additional stress in the embankment changes from “parabolic single peak” to “double peak” distribution, as indicated by the rockfall rebound in the model test, and the change suggests an increase in structural stiffness. With the increase of impact times, the tensile property

and lateral restraint effect of the reinforcement material cause the stiffness increase of the prestressed reinforced embankment far greater than that of the plain fill embankment, resulting in fewer impact times corresponding to the rockfall rebound under the former condition. The additional stress near the impact point is the largest, which is consistent with the maximum reinforcement material strain near the impact point.

(3) The rockfall impact duration in the prestressed reinforced soil embankment is shorter than that in plain fill embankment, and the duration distribution in the prestressed reinforced soil embankment is more uniform. The prestressed reinforced technique causes the reinforcement material exhibits its tensile property in advance, pre-eliminating the compression of the filling material and improving the stiffness of the reinforced embankment, which promotes upper impact load diffusion and its uniform transmission to the lower subgrade. The duration decreases with the increase of the distance from the impact point.

(4) With the increase of impact times, the deformation of the reinforcement material presents a trend of "first rise and then decline", and the internal impact transmission ratio in the prestressed reinforced embankment also presents a trend of "first rise and then decline". The reinforcement material deformation is the most important factor determining the embankment deformation. When the reinforcement material deformation increases considerably, the distance between the impact point and pressure measuring point decreases, causing the transmission ratio to rise. When the reinforcement material deformation is stabilized, the constraint effect on the embankment filling material is maximized, and the embankment stiffness is maximized. The energy dissipation mode changes from deformation absorption to outward diffusion, and the diffusion range continues to increase, resulting in a decrease in transmission ratio.

The prediction equations for pit sizes and impact times based on the Levenberg-Marquardt optimization algorithm cannot be quantitatively and directly applied to full-scale tests or actual projects, but they can be employed to obtain reliable and accurate prediction equations by real-time updating parameter values, which is helpful for hazard assessment and early warning in areas with a high incidence of rockfall hazards.

References

[1] HUNGR O, LEROUEIL S, PICARELLI L. The Varnes classification of landslide types, an update[J]. Landslides, 2014, 11(2): 167−194.

[2] JI Zhong-min, TANG Yi-ju, WU Fa-quan, et al. Laboratory investigation of the effect of rockfall shape and size on coefficient of restitution[J]. Rock and Soil Mechanics, 2021, 42(3): 665−672.

[3] HUANG Bo-lin, YIN Yue-ping, LI Bin, et al. Simplified numerical model and verification for the impulse wave generated by situated collapse of a dangerous columnar rock mass[J]. Rock and Soil Mechanics, 2021, 42(8): 2269−2278.

[4] KUMAGAI Y, KUBO T, YOSHIDA M. Rock-fall protection wall using reinforced soil structure affected by the 2011 off the Pacific coast of Tohoku earthquake[J]. Geosynthetics Engineering Journal, 2011, 26: 77−82.

[5] PAIXÃO A, FORTUNATO E, CALÇADA R. The effect of differential settlements on the dynamic response of the train–track system: a numerical study[J]. Engineering Structures, 2015, 88(1): 216−224.

[6] ZHENG Jun-jie, FU Hai-ping, CAO Wen-zhao, et al. Investigation of the calculation method of efficacy for geogrid-reinforced pile-supported embankments[J]. Journal of Huazhong University of Science and Technology (Natural Science Edition), 2017, 45(8): 64−68, 80.

[7] YANG Guang-qing, DU Xue-ling, ZHOU Qiao-yong, et al. Field tests on behaviors of geogrid reinforced lime treated soil retaining walls[J]. Chinese Journal of Geotechnical Engineering, 2010, 32(12): 1904−1909.

[8] LIU Hua-bei. Reinforcement loads of geosynthetic- reinforced soil retaining walls under horizontal earthquake loading[J]. Chinese Journal of Geotechnical Engineering, 2022, 44(2): 288−294.

[9] NIU Xiao-di, YANG Guang-qing, WANG He, et al. Field tests on structural properties of reinforced retaining walls with different panels[J]. Rock and Soil Mechanics, 2021, 42(1): 245−254.

[10] SHINODA M, UCHIMURA T, TATSUOKA F, et al. A new simple method to substantially increase the seismic stability of reinforced soil structures[J]. Soil Dynamics and Earthquake Engineering, 2002, 22: 1115−1123.

[11] SIMMONS M, POLLAK S, PEIRONE B. High energy rock fall embankment constructed using a freestanding woven wire mesh reinforced soil structure[C]//Proceedings of the 60th Highway Geology Symposium. Buffalo. New York: [s. n.], 2009: 290−301.

[12] RIMOLDI P, LORIZZO R, PETTINAU D, et al. Impressive reinforced soil structures in Italy[C]//Proceedings of the 1st Pan American Geosynthetics Conference. Cancun, Mexico: [s. n.], 2008: 789−798.

[13] LORENTZ J, PLASSIARD J P, MUQUET L. An innovative design process for rockfall embankments: application in the protection of a building at Val d'Isère[C]// Proceedings of the 3rd Euro Mediterranean Symposium on Advances in Geomaterials and Structures - AGS 2010. Djerba, Tunisia: [s. n.], 2010: 277−282.

[14] BRUNET G, GIACCHETTI G, BERTOLO P. Protection from high energy rockfall impacts using Terramesh embankment: design and experiences[C]//Proceedings of the 60th Highway Geology Symposium. New York: [s. n.], 2009: 107−124.

[15] LACKNER C, BERGADO D T, SEMPRICH S. Prestressed reinforced soil by geosynthetics-concept and experimental investigations[J]. Geotextiles and Geomembranes, 2013, 37(4): 109−123.

[16] TATSUOKA F, UCHIMURA T, TATEYAMA M, et al. Creep deformation and stress relaxation in preloaded/ prestressed geosynthetic-reinforced soil retaining walls[C]// Proceedings of ASCE'96Measuring and Modeling Time-Dependent Soil Behavior, ASCE Washington Convention. [S. l.]: [s. n.], 1996: 228−278.

[17] SHINODA M, UCHIMURA T, TATSUOKA F, et al. A new simple method to substantially increase the seismic stability of reinforced soil structures[J]. Soil Dynamics and Earthquake Engineering, 2002, 22(9−12): 1115−1123.

[18] ROH H S, TATSUOKA F. Effects of preloading and prestressing on the strength and stiffness of geosynthetic reinforced clay in plane strain compression[J]. Geosynthetics International, 2002, 8(5): 393−444.

[19] SHIVASHANKAR R, JAYARAJ J. Behaviour of prestressed geosynthetic reinforced granular beds overlying weak soil[J]. Indian Geotechnical Journal, 2014, 44(1): 26−38.

[20] JAYAMOHAN J, SHIVASHANKAR R. Some studies on prestressed reinforced granular beds overlying weak soil[J]. ISRN Civil Engineering, 2012, 2012: 436327.

[21] LOVISA J, SHUKLA S K, SIVAKUGAN N. Behaviour of prestressed geotextile-reinforced sand bed supporting a loaded circular footing[J]. Geotextiles and Geomembranes, 2010, 28(1): 23−32.

[22] DU Yun-xing, SHANG Shou-ping, ZHOU Fen. Technical principle of prestressed CFRP reinforced soil[J]. Journal of Central South Highway Engineering, 2005, 30(1): 29−32.

[23] KUWANO J, TACHIBANA S, ISHIGAKI T. Confined-reinforced subgrade to reduce differential settlement of road pavement[C]//Proceedings of 5th KGS-JGS Geotechnical Engineering. Seoul, Korean: [s. n.], 2013.

[24] OHTA H, ISHIGAKI T, TATTA N. Retrofit technique for asphalt concrete pavements after seismic damage[C]// Proceedings of the 18th International Conference on Soil Mechanics and Geotechnical Engineering. Paris: [s. n.], 2013: 1333−1336.

[25] HUNG H M, KUWANO J, TACHIBANA S. Effect of prestress in geogrid on stiffness of confined-reinforced earth[J]. Geosynthetics Engineering Journal, 2015, 30: 31−36.

[26] WANG Zhi-jia, LI Sheng-min, HE Xu, et al. System similar design method for shaking table test based on separated dimensional analysis and its application in soil–underground pipe gallery interaction[J]. Chinese Journal of Rock Mechanics and Engineering, 2021, 40(12): 2553−2569.

[27] LU Liang, ZHANG Yue-chen, WANG Zong-jian, et al. Study on impact stress distribution of ground reinforced embankments under rockfall impact[J]. Chinese Journal of Rock Mechanics and Engineering, 2021, 40(5): 997−1008.

[28] MARQUARDT D W. An algorithm for least-squares estimation of nonlinear parameters[J]. Journal of the Society for Industrial and Applied Mathematics, 1963, 11(2): 431−441.

[29] SUN He-xuan, PEI Dong-xing, ZHI Hui-qiang, et al. Magnetic moment calculation method based on magnetic gradient tensor and Levenberg-Marquardt optimization[J]. Chinese Journal of Sensors and Actuators, 2021, 34(1): 64−69.

[30] KAWAHARA S, MURO T. Effects of dry density and thickness of sandy soil on impact response due to rockfall[J]. Journal of Terramechanics, 2006, 43(3): 329−340.

[31] KAWAHARA S, MURO T. Effects of weight mass and drop height on vertical distribution of dry density of sandy soil in one-dimensional impact compaction[C]//Proceedings of the 5th Asia-Pacific Regional Conference of the ISTVS. [S. l.]: [s. n.], 1998: 151−161.

[32] SU Yu-chen, WANG Yuan, TANG Hui-ming, et al. Macro-mesoscopic investigation of cushioning mechanism of recycled concrete aggregate under successive rockfall impacts[J]. Rock and Soil Mechanics, 2022, 43(10): 2698−2706.

[33] LU L, LIN H, WANG Z, et al. Experimental and numerical investigations of reinforced soil wall subjected to impact loading[J]. Rock Mechanics and Rock Engineering, 2021, 54(11): 5651−5666.